

Efficient, Wide Angle, Structure Tuned 1×3 Photonic Crystal Power Splitter at 1550 nm for Triple Play Applications

Din Chai Tee, Toshio Kambayashi, Seyed Reza Sandoghchi, Nizam Tamchek, and Faisal Rafiq Mahamd Adikan

Abstract—We propose a wide angle, efficient and low loss 1×3 power splitter based on triangular lattice air holes silicon slab Photonic Crystal (PhC). Desired power splitting ratio was achieved by altering the structure at the junction area of the power splitter. Simulation results obtained using 2-D finite difference time domain method show that for TE polarization incident signal, the power is distributed almost equally with total normalized transmission of 99.74% and negligible reflection loss at the 1550 nm optical operating wavelength. In addition, the power splitter can operate at 1388 nm and 1470 nm optical wavelengths.

Index Terms—Finite difference method, optical devices, optical tuning, photonic crystal.

I. INTRODUCTION

PHOTONIC CRYSTAL (PhC) is a low loss structure which the refractive index of its different materials alternates periodically. PhC devices work based on both bandgap theory for guiding light in one direction, and total internal reflection to confine light in the other direction. Using the two mechanisms, the scattering loss induced by wall roughness in conventional planar waveguides [1] can be minimized. In addition, successful signal propagation through 90 degree sharp bend or any degree of bending in PhC was shown both theoretically and experimentally [2]–[4].

In general, there are two types of PhC slabs. The first is dielectric rods in air, which shows a transverse magnetic (TM) bandgap, and the second is air holes in dielectric slab that exhibits transverse electric (TE) bandgap [5]. In terms of fabrication difficulty, air hole slab is much easier to fabricate and is more reliable for practical applications. PhC devices fabricated by dielectric rods in air, in contrast, induce more out of plane

losses due to the insufficient vertical confinement by total internal reflection. Some researchers apply high-index segments in the dielectric rods leading to vertical confinement, resulting in extremely low out of plane losses in the PhC waveguides [6]. However, this adds to fabrication complexity.

PhC has emerged as an important enabling key for future compact optical integrated devices. They include basic optical components such as power splitters [7], directional couplers [8], and optical filters [9]. Theoretically, PhC based components should have nearly zero reflection and 100% transmission. However, practical devices are limited by fabrication accuracies.

PhC slab based 1×2 power splitter, or Y-branch power divider, has been demonstrated and fabricated by many research groups since a decade ago [4], [7], [10]–[13]. However, recently, there have been growing interests in 1×3 PhC power splitters, enabling triple play capabilities for example. By applying multimode interference (MMI) technique [14], or coupling [15], [16], researchers have been able to demonstrate 1×3 power splitter theoretically and experimentally. In the work reported by Zhang *et al.* [14], the optimum normalized transmittance calculated through simulation is around -7.5 dB for each branch at 1567.4 nm wavelength and the experimental results show values around -10 dB for each branch at 1550 nm. Such a high transmission loss is not desirable for efficient photonic integrated devices. Another problem for MMI devices is the considerable small output splitting angle which limits its application. In a separate work, a power splitter based on dielectric rod in air was fabricated by Liu [15], which shows the transmission loss of 10%. However, the device is not suitable for optical communication because of its operating wavelength in the visible range (532 nm). In another attempt, a 1×3 power divider based on ring resonators and directional couplers has been reported by Djavid *et al.* [16] which shows 99% transmission. Using dielectric rods in air, they obtained about 33% normalized transmission for each of the three branches at operating wavelength of 1594 nm through the coupling between the waveguide and the ring resonators. In relation to this coupling technique, the size of the PhC will become longer due to the required interaction length for complete transfer of the propagating electromagnetic wave from one waveguide to another. Therefore, such a design may not fulfill the high integration requirement for compact optical integrated devices.

Beside the aforementioned MMI and coupling methods, modification of PhC structure can result in 1×3 power splitters. In this manuscript, a structure tuning method for a 1×3

Manuscript received December 04, 2011; revised May 14, 2012; accepted June 04, 2012. Date of publication June 20, 2012; date of current version August 17, 2012. The work was supported in part by MOHE High Impact Research under Grant A000007-50001.

D. C. Tee, S. R. Sandoghchi, and F. R. Mahamd Adikan are with the Photonics Research Group, Department of Electrical Engineering, University of Malaya, 50603 Kuala Lumpur, Malaysia (e-mail: tdchai123@gmail.com; rezasandoghchi@gmail.com; rafiq@um.edu.my).

T. Kambayashi is with the Department of Electrical Engineering, Nagaoka University of Technology, Niigata 940-2188, Japan (e-mail: toshikam@vos.nagaokaut.ac.jp).

N. Tamchek is with the Department of Physics, University Putra Malaysia, 43400 Serdang, Selangor, Malaysia (e-mail: nizamtm@gmail.com).

Color versions of one or more of the figures in this paper are available online at <http://ieeexplore.ieee.org>.

Digital Object Identifier 10.1109/JLT.2012.2205369

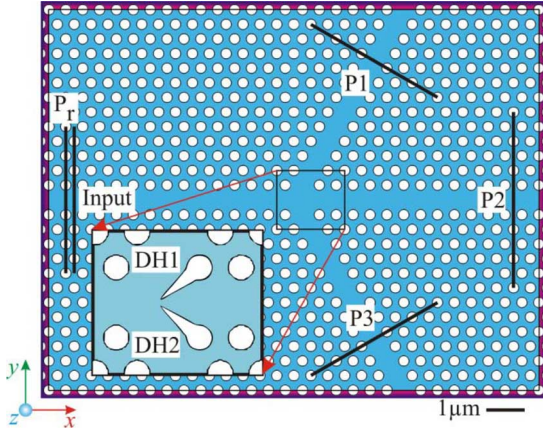


Fig. 1. Basic 1×3 power splitter. Zoom-in box shows the modified power splitter with drop holes DH1 and DH2 at the junction area.

PhC slab based power splitter is proposed and the results are verified by numerical simulation. This paper is organized as follows. Section II describes the design and parameters used for the proposed splitter. In Section III, the simulation results and discussion are presented. And finally, conclusion and future works are presented in Section IV.

II. DESIGN AND PARAMETERS

A basic PhC slab based power splitter with triangular lattice air holes is shown in Fig. 1. It consists of a Y branch with 120 degree angle and a waveguide connected at the junction. Generally, the waveguides are similar, and the signal is input from the position indicated in Fig. 1. The output power for each of the branches are measured at the locations shown in the same figure, where P1, P2, and P3 are the transmission powers at the upper, middle, and lower output branches respectively. Moreover, the reflection loss, P_r , is measured at half lattice distance before the input signal excitation location, and P_{total} , is the measure of total input power, indicating the amount of power entered into the structure and distributed within it [14].

The modified power splitter is shown in the zoom-in box in Fig. 1 where the design has been changed at the junction area of the branches by including two drop holes (DH1 and DH2). The layout of the drop hole is shown in Fig. 2. The drop holes are designed to interact with the incoming electromagnetic wave while they reduce the reflection loss and guide the wave into the branches effectively [13]. The main parameters of the drop hole are $r1$, L , and θ , where $r1$ is the radius of the drop hole, L is the length from center of drop hole to the sharp corner, and θ is the bending angle, with positive θ for upward bending and negative θ for downward. In the layout shown in Fig. 2, r indicates air hole radius. In the simulation, DH1 is bent downward ($-\theta$) and DH2 is bent upward ($+\theta$), which means that the two drop holes are approaching each other or crossing each other depending on the degree of bending and the drop hole's length. Any changes in $r1$, L and θ will either affect the reflection loss or power splitting ratio or both at the same time.

In this work, a 2-D finite difference time domain (FDTD) method has been used for analyzing the proposed device. For the simulation, the effective refractive index of the PhC slab

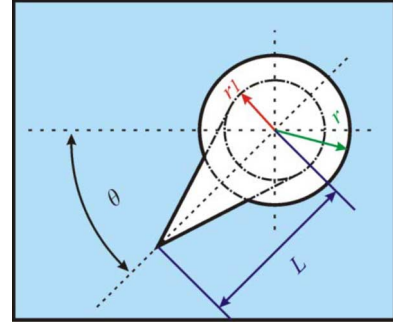


Fig. 2. Layout of the drop hole used in the 1×3 power splitter.

with holes is calculated using the effective index method [17]. Moreover, air hole radius of $r = 135$ nm, lattice constant of $\Lambda = 440$ nm, and slab-effective refractive index of 2.9 corresponding to 240 nm thick silicon on silica substrate operating at 1550 nm wavelength are used [8]. The aforementioned effective index is applicable for other wavelengths as well [8]. As 2-D method is used in the simulation, the out of plane losses are fully ignored. Detailed study showed that the magnitude of these losses is very low [18].

The PhC slab is on the x-y plane, with the z axis pointing out of plane. The input signal propagates along the x-axis. The 2-D FDTD mesh size used in this simulation are $\Delta x = \Delta y = 10$ nm. The time step, Δt is obtained from Courant limit and is equal to 2.3×10^{-17} seconds. We have used 200 000 iterations for the FDTD computation to obtain the steady-state result. The overall size of splitter is about $13 \mu\text{m} \times 10 \mu\text{m}$, and it can be further reduced because the structure is only altered at the junction area. Its small size makes it promising for the future compact photonic integrated optical devices.

A finite computation region with general Neumann or Dirichlet boundary conditions causes the propagating electromagnetic wave to be reflected back at the boundary of computational region. Therefore, a 22 layer Berenger perfectly match layer (PML) [19] is applied at the boundary regions to absorb the entire outward propagating electromagnetic wave. TE polarization has been used for the simulation with its magnetic field only in the z direction (H_z), and, the electric field in both x and y directions (E_x and E_y).

III. RESULT AND DISCUSSION

To evaluate the advantages of the proposed structure, the basic power splitter without drop holes is simulated and compared with the proposed splitter using the aforementioned parameters.

By filling a row of air holes, a waveguide is created that can support only single-mode propagation. The steady-state of z-component of magnetic field (H_z) is shown in Fig. 3. The fluctuation in magnitude of the field is due to higher confinement near the channel's adjacent holes and less confinement in the areas between the holes. Measured powers are normalized with respect to P_{total} . The basic structure has high reflection loss and unequal normalized output transmission at each branch. The wide splitting space at the junction area causes the incoming single-mode electromagnetic wave to transform

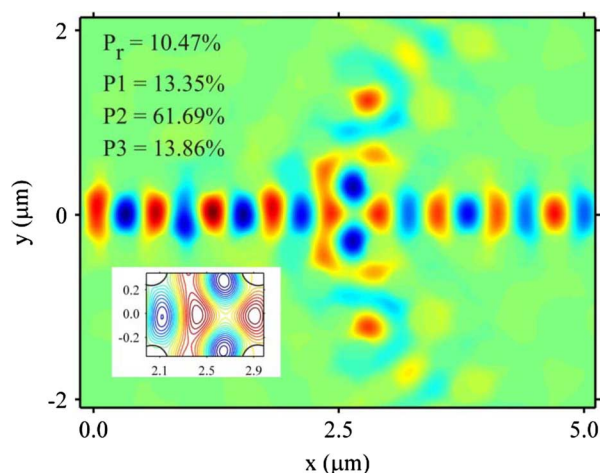


Fig. 3. Basic power splitter design. Normalized output transmission and reflection powers are shown at the top left corner in the figure. The inset shows the contour plot at the junction area.

into multimode. The mono-mode branches thus experience mismatch with the incoming multimode electromagnetic wave and therefore, a considerable portion of power is lost due to reflection and dispersion.

In the proposed design, drop holes are utilized to reduce the waveguide space at the junction area and consequently to prevent the multimode propagation and mismatch from occurring. Besides, parameters of the drop holes, can alter and match the impedance of waveguides, and consequently result in equal distribution of the incoming single-mode wave into three single-mode waves propagating in the branches.

Palamaru *et al.* [20] showed that a tiny hole, followed by a line of holes in a gradually increasing size manner, could adiabatically convert conventional waveguide mode into a PhC waveguide mode to achieve mode matching without incurring significant loss. The concept is verified experimentally by Wilson *et al.* [13]. Besides, impedance matching between output channels and input channel reduces the reflected wave and increases the power transmission efficiency. By adding extra holes to the input channel, intrinsic impedance can be tuned to achieve almost perfect impedance matching [21]. In order to split the power equally among the output channels with very low reflection, the branches' impedance should be similar and should match with input channel [21]. Optimization for the splitter is done by tuning one of the parameters while the other two are fixed. Repeating the procedure for other parameters (if required) can disclose a local optimized region. First, the radius of the drop, $r1$, and the bending angles, θ and $-\theta$ are fixed, while the effect of drop's length is studied. The result shown in Fig. 4 indicates that for the length size within 2.2Λ to 2.4Λ , the normalized output transmission is divided equally on each output port, with the optimum length occurring at $L = 2.3\Lambda$. Further optimizations were not necessary. The layout for the drop hole length at $L = 2.3\Lambda$ is shown in the inset. With the current technology, fabrication of holes with accuracy up to 15 nm has been achieved using focused ion beam method [22]. The smallest dimension in the drop hole which is equal to the mesh size used in this simulation is 10 nm which will be viable

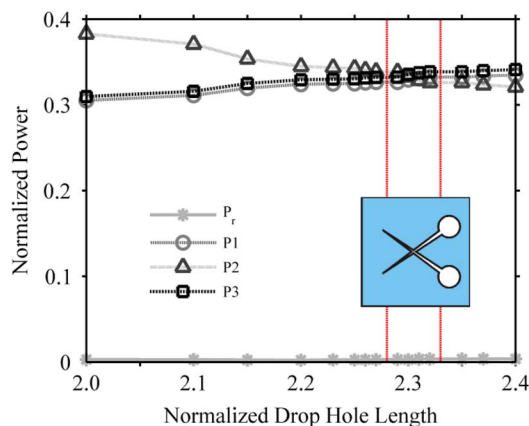


Fig. 4. Normalized output transmission and reflection power versus drop hole length L normalized with respect to lattice constant Λ at $r1 = 0.25r$ and $\theta = \pm 35^\circ$. The interval between the vertical red lines indicates the optimum operation region. The optimum region is calculated based on the computation accuracy of the simulation. The inset shows the layout of the drop holes at $L = 2.3\Lambda$.

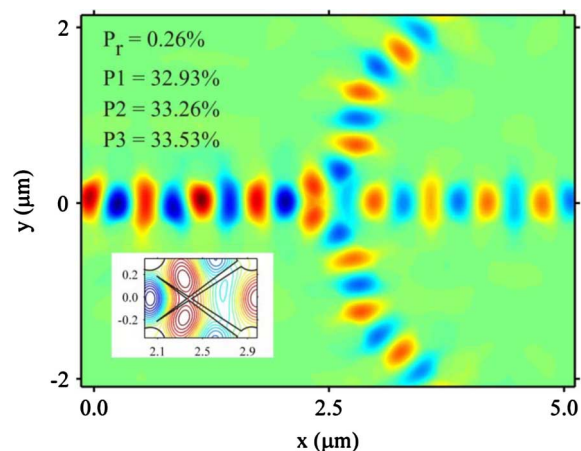


Fig. 5. Steady-state magnetic field (H_z) distribution at $L = 2.3\Lambda$, $r1 = 0.25r$ and $\theta = \pm 35^\circ$ at 1550 nm wavelength. The inset shows the contour plot at the junction area.

with a slight improvement in the aforementioned fabrication technology.

Steady-state magnetic field (H_z) distribution at point $L = 2.3\Lambda$, $r1 = 0.25r$, and $\theta = \pm 35^\circ$ is shown in Fig. 5 indicating a desirable field separation into the branches. The multimode behavior at the junction area has been suppressed by the drops showing a good impedance matching between channels, leading to a considerable reduction in reflection and dispersion loss. The normalized transmitted power at P1 is 32.93%, at P2 is 33.26%, and at P3 is 33.53%, while the reflection loss is as low as 0.26%, which is quite negligible. The slight asymmetry in output power P1 and P3 is due to the possibility that the discretization mesh used in the simulation do not share the central axis of symmetry with the structure. Therefore, there is a 0.6% of tolerance in the calculated output powers. This suggests an interval (a region) of optimum operation highlighted in Fig. 4. Within the interval, the normalized power transmission is nearly 33% for all output branches. For $L = 2.3\Lambda$, $r1 = 0.25r$, and $\theta = \pm 35^\circ$ the structure shows the best symmetry within the region. Compared with

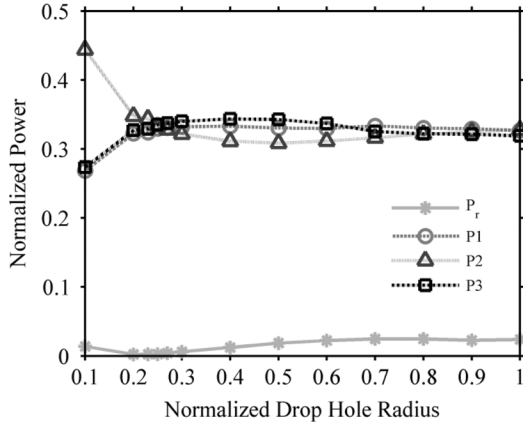


Fig. 6. Normalized output transmission and reflection power versus drop hole radius $r1$, normalized with respect to air hole radius r , at $L = 2.3\lambda$ and $\theta = \pm 35^\circ$.

the work reported in [14], our design shows better performance for power transmission at 1550 nm.

The parameters of drop holes within the local optimum operating region are feasible for fabrication. From the results, the drop hole length for the proposed slab can be varied between 1003 nm and 1025 nm. In order to show the flexibility of the fabrication parameters for the proposed splitter, the sensitivity of the design to the other parameters are studied, as follows.

While the drop's length at $L = 2.3\lambda$ and bending angles at $\theta = \pm 35^\circ$ are fixed, the drop's radius, $r1$, is changed. The result, shown in Fig. 6, indicates that while radius is changing from $r1 = 0.2r$ to $r1 = 0.3r$, the average reflection is negligible, and is about 0.33%, while the normalized output transmission is almost equal for all branches. This allows for a $\pm 20\%$ tolerance in drop's radius for fabrication of the drop holes. The effect of drop's radius in reflection loss is explained by waveguide input impedance that is altered by drop's parameters. Increase in drop's radius decreases the local effective index experienced by the incoming electromagnetic wave and thus increases the impedance mismatch. Therefore, more light is reflected back toward the input direction and consequently reflection loss increases. In contrast, as $r1$ reduces ($< 0.2r$), DH1 and DH2 become smaller in size, and the device starts to behave like the basic power splitter as shown in Fig. 1, with most of the output signal intensity flowing into the direction of P2.

Study of the bending angles shows that, while the drop's length is fixed at $L = 2.3\lambda$ and drop's radius at $r1 = 0.25r$, for the bending degree from $\theta = \pm 30^\circ$ to $\theta = \pm 36^\circ$, the normalized output transmission for each branch is within $33\% \pm 1\%$ with low reflection. This is depicted in Fig. 7. Also, this tolerance in bending angle, θ , adds extra advantage in fabrication of drop holes and thus the splitter. Fig. 8 shows the field distribution at bending angles of 25° , 35° and 45° . Fig. 8(a) represents the fields amplitude for the corresponding yellow dash-dot line in Fig. 8(b). It shows that the magnetic field is continuous, while electric field and power are discontinuous across the drop hole (low index region). This discontinuity is due to the fact that the electric displacement field requires to be continuous across the index contrast interface. Light confinement in low index material region of sub-wavelength size can be achieved by the dis-

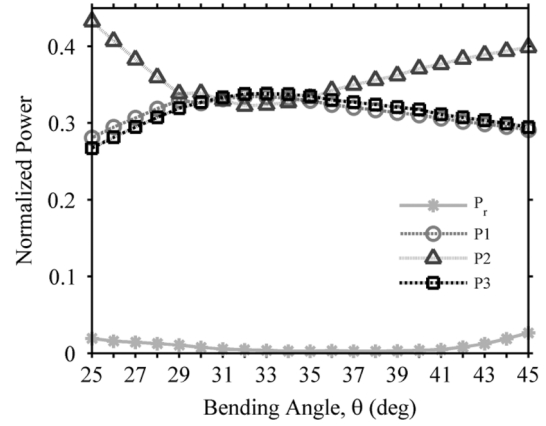


Fig. 7. Normalized output transmission and reflection power versus bending angle θ at $L = 2.3\lambda$ and $r1 = 0.25r$.

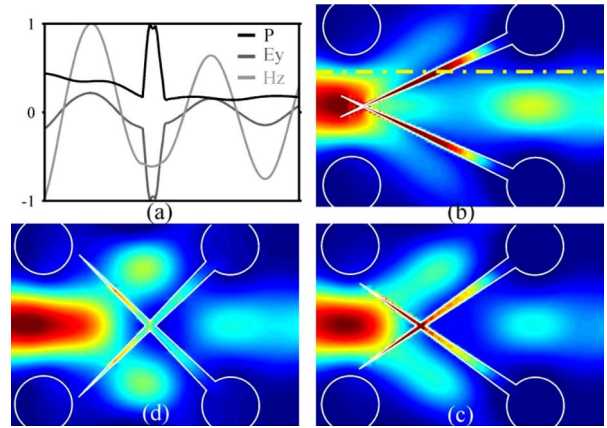


Fig. 8. Field distribution for different bending angles. (a) Field amplitude corresponding to the dash-dot line (yellow) in (b), where P is the power, E_y is the y-component of the electric field vector and H_z is z-component of the magnetic field vector. Power distribution (b) at bending angle of 25° , (c) at bending angle of 35° , and (d) at bending angle of 45° .

continuity of electric field perpendicular to the index contrast interface. The confinement of light power in the drop holes, as shown in Fig. 8(b)–(d), is due to both E_y and E_x distributions. Naturally, larger E_y values correspond to a larger transmittance into the center branch and E_x to the upper and lower branches. By introducing drop holes, the E_y and E_x distribution is altered and simulation result indicates that at certain range of drop's bending angles, the transmitted powers to the branches are similar. This is possibly due to the fact that, within the aforementioned bending range, the power is trapped and guided in the drop holes, and distributes equally to all branches. In contrast, more power flows into the P2 direction as the bending angle is outside of the range mentioned above. This possibly can describe the impedance matching caused by altering the bending angle.

Fig. 9 shows the normalized output transmission and reflection power for a chosen optimum parameters with respect to different wavelengths. The graph shows that the power splitter can effectively operate at two other wavelengths as well. The first wavelength is 1388 nm, which is in the E-band of the optical communication spectrum. The second wavelength is 1470 nm, which is in the S-band of the spectrum. Having this,

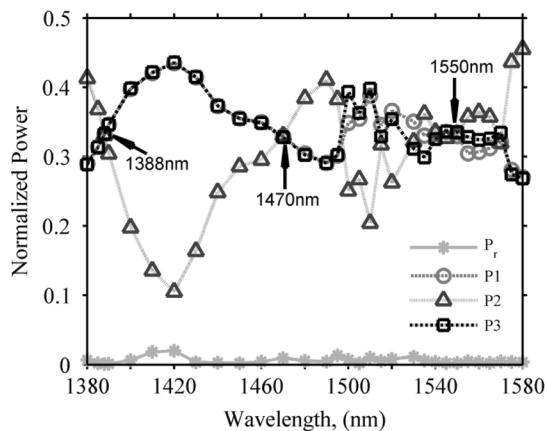


Fig. 9. Normalized output transmission and reflection power versus wavelength at $L = 2.3\lambda$, $r1 = 0.25r$ and $\theta = \pm 35^\circ$.

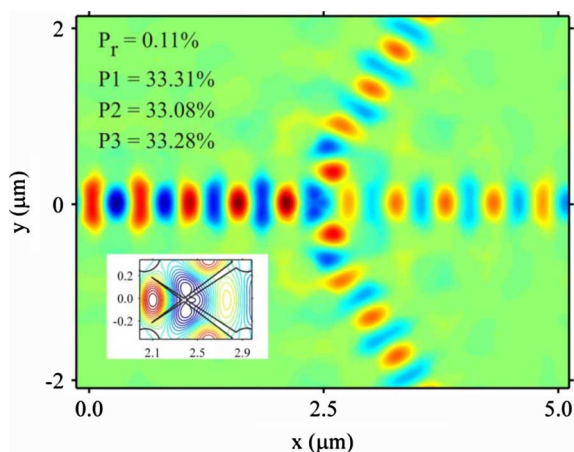


Fig. 10. Steady-state magnetic field (H_z) distribution for $L = 2.3\lambda$, $r1 = 0.25r$ and $\theta = \pm 35^\circ$ at 1388 nm wavelength. The inset shows the contour plot at the junction area.

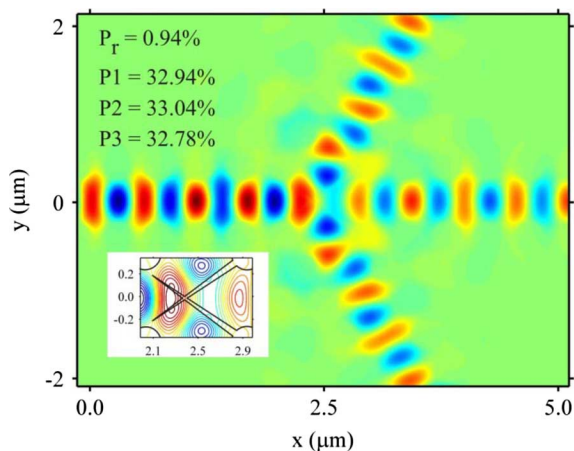


Fig. 11. Steady-state magnetic field (H_z) distribution for $L = 2.3\lambda$, $r1 = 0.25r$ and $\theta = \pm 35^\circ$ at 1470 nm wavelength. The inset shows the contour plot at the junction area.

we can operate the splitter at three different optical communication spectrums to suit certain applications. This multiple operating wavelengths feature has not been reported before.

The steady-state magnetic fields for the 1388 nm and 1470 nm wavelengths are shown in Figs. 10 and 11.

Fig. 10 shows a reflection loss as low as 0.11%, obtained when 1388 nm wavelength is used for the simulation. The normalized output transmission is 33.31% at P1, 33.08% at P2, and 33.28% at P3. From Fig. 11, the normalized output transmission for the three branches at 1470 nm wavelength is about 33% and the structure has slightly higher reflection loss of 0.94%. Channel waveguides created based on photonic bandgap principle can support single mode behavior over a wide range of wavelengths. However, different wavelengths may experience different transmittance. In the proposed splitter, similar transmittance has been demonstrated for 1388 nm and 1470 nm wavelengths in addition to 1550 nm, opening the potential for triple play applications.

IV. CONCLUSION

In this study, a power splitter was proposed by modifying the lattice structure in which two drop holes were introduced at the junction. Based on the results, the structure is capable of dividing the electromagnetic wave power desirably, i.e., $\sim 33\%$ at each branch with a very negligible reflection loss, at operating wavelength of 1550 nm. Besides, it was shown that this splitter is capable of operating at two other important optical communication bands, E-band and S-band, with desirable power splitting ratio and low reflection loss.

ACKNOWLEDGMENT

The authors would like to thank K. Matsunaga for his technical help.

REFERENCES

- [1] J. M. Elson, "Propagation in planar waveguides and the effects of wall roughness," *Opt. Exp.*, vol. 9, pp. 461–475, 2001.
- [2] A. Chutinan and S. Noda, "Waveguides and waveguide bends in two-dimensional photonic crystal slabs," *Phys. Rev. B*, vol. 62, pp. 4488–4492, 2000.
- [3] S. Olivier, H. Benisty, M. Rattier, C. Weisbuch, M. Qiu, A. Karlsson, C. J. M. Smith, R. Houdre, and U. Oesterle, "Resonant and nonresonant transmission through waveguide bends in a planar photonic crystal," *Appl. Phys. Lett.*, vol. 79, pp. 2514–2516, 2001.
- [4] S. Foghani, H. Kaatuzian, and M. Danaie, "Simulation and design of a wideband T-shaped photonic crystal splitter," *Optica Applicata*, vol. XL, pp. 865–872, 2010.
- [5] S. G. Johnson, P. R. Villeneuve, S. Fan, and J. D. Joannopoulos, "Linear waveguides in photonic-crystal slabs," *Phys. Rev. B*, vol. 62, pp. 8212–8222, 2000.
- [6] A. A. M. Kok, J. J. G. M. van der Tol, R. Baets, and M. K. Smit, "Reduction of propagation loss in pillar-based photonic crystal waveguides," *J. Lightw. Technol.*, vol. 27, no. 17, pp. 3904–3911, Sep. 2009.
- [7] N. Nozhat and N. Granpayeh, "Analysis and simulation of a photonic crystal power divider," *J. Appl. Sci.*, vol. 7, pp. 3576–3579, 2007.
- [8] I. Park, H. S. Lee, H. J. Kim, K. M. Moon, S. G. Lee, B. H. O. S. G. Park, and E. H. Lee, "Photonic crystal power-splitter based on directional coupling," *Opt. Exp.*, vol. 12, pp. 3599–3604, 2004.
- [9] Z. Zhang, M. Dainese, L. Wosinski, S. Xiao, M. Qiu, M. Swillo, and U. Anderson, "Optical filter based on two-dimensional photonic crystal surface-mode cavity in amorphous silicon-on-silica structure," *Appl. Phys. Lett.*, vol. 90, pp. 041108–041110, 2007.
- [10] L. J. Kauppinen, T. J. Pinkert, H. J. W. M. Hoekstra, and R. M. de Ridder, "Photonic crystal cavity-based Y splitter for mechano-optical switching," *IEEE Photon. Technol. Lett.*, vol. 22, no. 13, pp. 966–968, Jul. 2010.
- [11] S. Y. Lin, E. Chow, J. Bur, S. G. Johnson, and J. D. Joannopoulos, "Low-loss, wide-angle Y splitter at ~ 1.6 μm wavelengths built with a two dimensional photonic crystal," *Opt. Lett.*, vol. 27, pp. 1400–1402, 2002.

- [12] L. H. Frandsen, P. L. Borel, Y. X. Zhuang, A. Harpoth, M. Thorhauge, M. Kristensen, W. Bogaerts, P. Dumon, R. Baets, V. Wiaux, J. Wouters, and S. Beckx, "Ultralow-loss 3-dB photonic crystal waveguide splitter," *Opt. Lett.*, vol. 29, pp. 1623–1625, 2004.
- [13] R. Wilson, T. J. Karle, L. Moerman, and T. F. Krauss, "Efficient photonic crystal Y-junctions," *J. Opt. A, Pure Appl. Opt.*, vol. 5, pp. S76–S80, 2003.
- [14] M. Zhang, R. Malureanu, A. C. Kruger, and M. Kristensen, " 1×3 beam splitter for TE polarization based on self-imaging phenomena in photonic crystal waveguides," *Opt. Exp.*, vol. 18, pp. 14944–14949, 2010.
- [15] C. Y. Liu, "Fabrication and optical characteristics of silicon-based two-dimensional wavelength division multiplexing splitter with photonic crystal directional waveguide couplers," *Phys. Lett. A*, vol. 375, pp. 2754–2758, 2011.
- [16] M. Djavid, A. Ghaffari, F. Monifi, and M. S. Abrishamian, "Photonic crystal power dividers using L-shaped bend based on ring resonators," *J. Opt. Soc. Amer. B*, vol. 25, pp. 1231–1235, 2008.
- [17] O. V. Ivanova, R. Stoffer, L. J. Kauppinen, and M. Hammer, "Variational effective index method for 3-D vectorial scattering problems in photonics: TE polarization," in *Proc. PIERS*, Moscow, Aug. 2009, pp. 1038–1042.
- [18] G. R. Hadley, "Out-of-plane losses of line-defect photonic crystal waveguides," *IEEE Photon. Technol. Lett.*, vol. 14, no. 5, pp. 642–644, May 2002.
- [19] J. P. Berenger, "A perfectly matched layer for the absorption of electromagnetic waves," *J. Computational Phys.*, vol. 114, pp. 185–200, 1994.
- [20] M. Palamaru and Ph. Lalanne, "Photonic crystal waveguides: Out-of-plane losses and adiabatic modal conversion," *Appl. Phys. Lett.*, vol. 78, pp. 1466–1468, 2001.
- [21] S. Boscolo, M. Midrio, and T. F. Krauss, "Y junctions in photonic crystal channel waveguides: High transmission and impedance matching," *Opt. Lett.*, vol. 27, pp. 1001–1003, 2002.
- [22] Y. Kurokawa, Y. Ohno, S. Kishimoto, T. Okazaki, H. Shinohara, and T. Mizutani, "Fabrication technique for carbon nanotube single-electron transistors using focused ion beam," *Jpn. J. Appl. Phys.*, vol. 43, pp. 5669–5670, 2004.

Din Chai Tee received the B.S. degree (with first-class honors) in telecommunication engineering from the University of Malaya, Kuala Lumpur, Malaysia, in 2010, where he is currently working toward the Ph.D. degree.

In 2010, he was selected to represent the University of Malaya to participant JENESYS (Japan-East Asia Network of Exchange for Students and Youths) exchange program at Nagaoka University of Technology, Niigata, Japan. He is currently a Research Assistant with the Flat Fibre Laboratory, Department of Electrical Engineering, University of Malaya, Kuala Lumpur, Malaysia. His current research interests include simulation on photonic crystal slab based devices, photonic crystal fiber, and development of novel Flat Fiber applications.

Toshio Kambayashi received the Ph.D. degree from the Tokyo Institute of Technology, Tokyo, Japan, in 1977.

He is currently a Professor with the Department of Electrical Engineering, Nagaoka University of Technology, Niigata, Japan, and is involved in research on optical waveguides, optical integrated circuits, and photonic crystal devices. From 1977 to 1979, he was a Lecturer with the Research Laboratory of Precision Machinery and Electronics, Tokyo Institute of Technology, where he was involved in the research of monolithically semiconductor laser fabrication for integrated optical circuits. He joined the Nagaoka University of Technology in 1979 as an Associate Professor. From 1981 to 1983, he was a Research Officer at the University of Bath, Bath, U.K., where his work involved the research of semiconductor lasers and LED's for integrated optical circuits.

Dr. Kambayashi is a member of the Institute of Electronics and Communication Engineers of Japan and the Japan Society of Applied Physics.

Seyed Reza Sandogchi received the B.S. degree (with first-class honors) in telecommunication engineering from the Sadjad Institute of Higher Education, Mashhad, Iran, in 2005, and the M.S. degree in telecommunication from University of Malaya, Kuala Lumpur, Malaysia, in 2011. His dissertation investigated the refractive index profile characterization methods.

His research mainly includes modeling and simulation of optical devices and developing characterization systems. He has been involved in establishment of fiber drawing facilities in University of Malaya, Kuala Lumpur, Malaysia, where he is currently working with the optical fiber fabrication team at the Flat Fibre Lab.

Nizam Tamchek received the B.S. degree in physics from Kanazawa University, Japan, in 2001, and the M.Sc. and Ph.D. degrees in photonics from the University of Malaya, Kuala Lumpur, Malaysia, in 2010.

He is currently a Lecturer with the Department of Physics, University Putra Malaysia. He joined the MCV D Laboratory at Telekom Research and Development in 2009. His work has focused on understanding the photonics device fabrication using FHD and MCV D system and development of photonics device for telecommunication and sensors.

Faisal Rafiq Mahamd Adikan received the Ph.D. degree from the Optoelectronics Research Centre, University of Southampton, Southampton, U.K., in 2007.

His Ph.D. work on flat fibre produced an international patent. He is currently the Head of the Photonics Research Group, University of Malaya, Kuala Lumpur, Malaysia, where he is involved with developing novel fabrication process to incorporate optically active materials into a glass matrix. He specializes in glass-based integrated optical devices for use in telecommunication and sensing applications. He has authored and coauthored more than 70 journal and conference papers on optics and engineering education.

Dr. Rafiq was the recipient of the Section Prize for the Best Engineering Research during Presentations at the House of Common (British Parliament) in 2006. He also received the SPIE Educational Scholarship in Optical Science and Engineering in 2004 and the Best Paper for Photonic Category during an international conference in 2003.